Published by IOP Publishing for Sissa Medialab

Received: *September 30, 2019*
Accepted: *December 11, 2019*
Published: *January 27, 2020*

21st International Workshop on Radiation Imaging Detectors
7–12 July 2019
Crete, Greece

Relative luminosity measurement with Timepix3 in ATLAS

B. Bergmann,[a,1] **T. Billoud,**[a,c] **P. Burian,**[a,b] **P. Broulim,**[b] **C. Leroy,**[c] **C. Lesmes,**[a,d] **P. Manek,**[a] **L. Meduna,**[a] **S. Pospisil,**[a] **A. Sopczak**[a] **and M. Suk**[a]

[a] *Institute of Experimental and Applied Physics, Czech Technical University in Prague Husova 240/5, 110 00 Praha 1, Czech Republic*
[b] *Faculty of Electrical Engineering, University of West Bohemia, Pilsen, Czech Republic*
[c] *Département de Physique, Université de Montréal, Montréal, QC, H3C 3J7, Canada*
[d] *Mathematical Engineering, Universidad EAFIT*

E-mail: benedikt.bergmann@utef.cvut.cz

Abstract: The capability of Timepix3 detectors installed in ATLAS to measure luminosity is evaluated. It is described how noisy pixels are identified and excluded. Two different methods for luminosity determination, i.e. cluster counting and thermal neutron counting are described and compared with each other. The achieved short-term relative precision with both methods is determined by modeling the luminosity curve. It is shown that using cluster counting a short-term relative precision of $< 0.5\,\%$ can be achieved for 60 s time intervals. For thermal neutrons, a short-term relative precision (for 60 s intervals) of $\approx 2\,\%$ was found. Hereby statistics was the limiting factor. The findings are discussed in view of Timepix3 upgrade plans for LHC Run-3.

Keywords: Beam-line instrumentation (beam position and profile monitors; beam-intensity monitors; bunch length monitors); Instrumentation for particle accelerators and storage rings - high energy (linear accelerators, synchrotrons); Hybrid detectors

[1] Corresponding authors.

https://doi.org/10.1088/1748-0221/15/01/C01039

Contents

1 Introduction

Medipix (Run-1) and Timepix (Run-2) pixel detector networks [1] installed in ATLAS have proven valuable for the characterization of the radiation fields, determination of the induced radioactivity [2], estimated dose rates at different places in the ATLAS experiment [3], and the measurement of luminosity [4–6]. In January 2018, four hybrid pixel detectors of Timepix3 [7] technology were added to the ATLAS-TPX network to gain operational experience with such devices in the ATLAS environment in view of the upcoming upgrade for ATLAS Run-3 [8]. Precise luminosity measurement is of paramount importance for the physics program of ATLAS. Luminosity uncertainty has often a direct impact on the error of cross-section determination. Moreover, precise knowlegde of luminosity is required for background level estimation for searches of new physics [9]. The Medipix/Timepix networks were installed as independent networks with the goal to provide complementary data for improvement of short-term luminosity measurement precision [9]. The presented paper reports studies on the capability of the newly installed Timepix3 devices for relative luminosity measurement.

We describe the Timepix3 network in ATLAS and methods currently used for luminosity determination with Medipix/Timepix detector (section 2), present a noisy pixel identification and removal (section 3) as a crucial first step of cleaning the data set for luminosity analysis and show how cluster and thermal neutron rates can be used to measure luminosity (section 4).

2020 JINST 15 C01039

2 Materials and methods

2.1 Timepix3 in ATLAS

Timepix3 [7] is the latest hybrid pixel detector developed by the Medipix3 collaboration. Timepix3 consists of a sensor layer flip-chip bump-bonded to the ASIC.[1] The sensor is divided into a square matrix of 256 × 256 pixels with a pixel pitch of 55 µm. It features simultaneous per pixel energy and time measurement (time granularity: 1.56 ns) in a data-driven (self-triggered) readout scheme. The per-pixel dead time amounts to 475 ns. Hit rates of 40 Mhits s^{-1} cm^{-2} can be achieved. The detectors used in this work were energy calibrated [10] and corrected for the time-walk effect [11].

Four Timepix3 detectors with 500 µ m thick silicon sensor layers were installed in the ATLAS experiment [8]. These were arranged in two stacks of two detectors facing each other. The device positions are summarized in table 1. All devices are synchronized with the LHC orbit clock and consequently with each other. Together with the good time resolution this allows measurements of the bunch structure of the LHC fills. Data are taken in 3-hour long acquisitions, which are interrupted by 5-15 s long dead time periods for reconfiguring the devices. This gives dead time to lifetime ratio of ≈ 0.4 %, which is considerably smaller than the ratio achieved by the ATLAS-TPX network (≈ 33 %). In the presented study, the inner two detectors are investigated (TPX4_A and TPX4_B), which started proper data taking at the end of April 2019. The data presented correspond to the center of mass energy $\sqrt{s}$ = 13 TeV proton-proton runs in the time period April 27, 2018 until the end of Run-2.

Table 1. Overview of the Timepix3 positions in ATLAS. *Green* color indicates devices whose data are presented.

Device name	Chip ID	X [mm]	Y [mm]	Z [mm]	Neutron converter
TPX3_4A	J04-W0036	-3,580	970	2,830	-
TPX3_4B	I04-W0036	-3,580	970	2,830	PE (fast), ^{6}Li (thermal)
TPX3_9A	I03-W0036	4,000	3,400	22,900	-
TPX3_9B	H03-W0036	4,000	3,400	22,900	-

2.2 Neutron detection

In order to achieve sensitivity to neutrons, one sensor (TPX3_4B) was equipped with neutron converters for detection of thermal (^{6}LiF) and fast neutrons (polyethylene, PE) [8]. The thermal neutron fluxes are determined through the ^{6}Li(n,α)^{3}H-reaction (940 barns, detection efficiency ≈ 1 %). Fast neutrons in the energy range from 1 MeV - 600 MeV can be seen through recoil protons below the PE region with a maximal detection efficiency of 0.3 % (around 16 MeV) [12, 13].

Figure 1 shows the effect of the neutron converter. Below ^{6}LiF an excess of so-called heavy blobs (large round clusters [14]) is seen. In figure 1(b), we compare the energy deposition spectra of the heavy blobs registered below the ^{6}LiF converter and the uncovered silicon region. The subtraction spectrum contains only the energy depositions by the ^{3}H emitted at 2.73 MeV and the

[1] Application specific integrated circuit.

2020 JINST 15 C01039

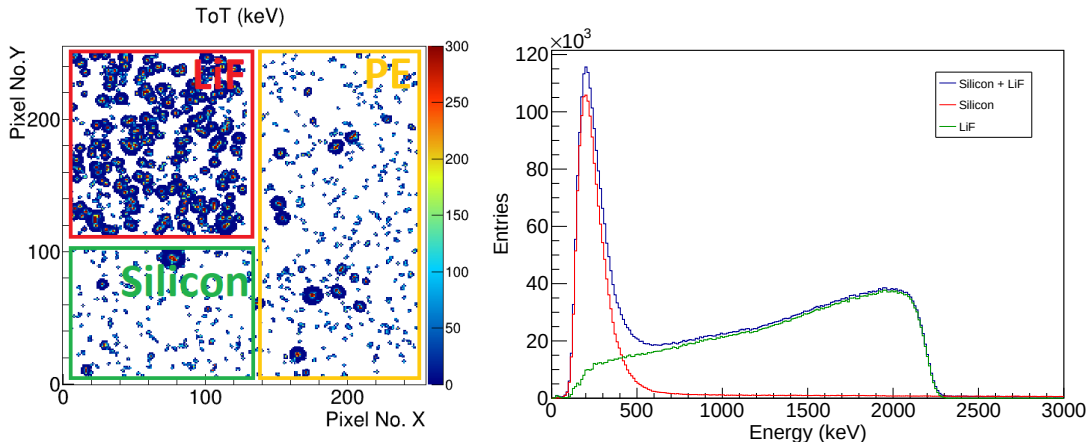

(a) (b)

Figure 1. Illustration of the thermal neutron converter effect. (a) Detector response in the form of heavy blobs. The different converter regions are marked. An excess can be seen below the ^{6}LiF-layer. The per-pixel energy deposition is color coded; (b) Comparison of the heavy blob energy spectra below the ^{6}LiF and the uncovered silicon region. The net converter effect is determined by subtracting the silicon signal from the signal below the ^{6}LiF region.

α-particle emitted at 2.03 MeV. Due to saturation of the pixel electronics and energy losses in the dead layer, not the full ^{3}H energy is measured. The thermal neutron fluxes are calculated by [12]:

$$\Phi_{\text{therm.}} = \frac{\frac{N_{\text{HB,LiF}}}{A_{\text{LiF}}} - \frac{N_{\text{HB,Si}}}{A_{\text{Si}}}}{\epsilon \times t}, \tag{2.1}$$

where $N_{\text{HB},i}$ is the number of heavy blobs, A_i is the area of region i. $\epsilon = 1\,\%$ (see [12] for the calibration procedure) is the converter efficiency and t is the acquisition time. The subtraction of the number of heavy blobs in the silicon (uncovered) region allows one to discard the heavy blobs created by the non-neutron radiation field.

2.3 Luminosity determination

Relative luminosity measurement with the Medipix and Timepix networks is done by scaling the pixel hit R_{hit} or cluster R_{cluster} rates with a calibration factor:

$$\mathcal{L} = C_i \times R_i,\ i \in \{\text{cluster}, \text{hit}\} \tag{2.2}$$

where the calibration factor C_i is determined during anchor runs by comparing the measured rates to reference luminosity values (provided e.g. by the Tile Calorimeter [15]) $C_i = \frac{\mathcal{L}_{\text{anchor},i}}{R_{\text{anchor},i}}$.

Cluster counting. uses the measured number of tracks generated by ionizing radiation in the sensor layer (clusters). Each individual cluster can be analyzed to determine the particle stopping power and other properties, which are used, e.g., for the measurement of the thermal neutron fluxes and the characterization of the radiation field(s) [4, 6]. In order to be able to reliably separate tracks, the matrix occupancy (number of triggered pixels within a frame) has to be kept low for avoiding significant track overlap. However, due to the high dead time of Medipix ($\tau_{\text{dead,MPX}} \approx 6$ s)

2020 JINST 15 C01039

and Timepix ($\tau_{\mathrm{dead,TPX}} \geq 0.33\,\mathrm{s}$), this causes an unfavorable ratio of detector life to dead time and reduces the achievable precision on short time scales.

Hit counting. was introduced to reduce the effect of the lifetime to deadtime ratio. In hit counting, the Medipix mode of the devices is used, where each pixel measures the number of interactions during the preset acquisition time (frame time). Since clusters do not have to be separated, long frame exposure times can be used. Depending on impact angle and energy, a single particle can trigger several pixels. The number of hits can be expressed as $N_{\mathrm{hits}} = \Sigma_{i=0}^{N_{\mathrm{clusters}}} S_i$, where S_i is the number of pixels in cluster i. For luminosity analysis, the number of interacting particles is estimated by dividing the measured number of hits by the average number of pixels per cluster (cluster size) S_{mean}: $\langle R_{\mathrm{hits,corr.}} \rangle = \frac{R_{\mathrm{hits}}}{\langle S_{\mathrm{mean}} \rangle}$. S_{mean} is determined in low luminosity runs, where even at long frame acquisition times no overlap is visible. The precision achieved in 10 s intervals was $\approx 0.1\,\%$ [16]. Compared to cluster counting, hit counting is inherently more affected by systematic uncertainties.

Timepix3 was designed for (almost) dead time free particle tracking, so that hit counting becomes obsolete. Thus, the presented work focuses on relative luminosity measurements with cluster counting methods. It should be noted, that by determining the calibration parameters during Van-der-Meer scans [17], absolute luminosity measurement could be done with Medipix/Timepix [18].

3 Noisy pixel identification and exclusion

During measurement in harsh radiation environment, pixel detectors can suffer from radiation damage, which is seen as soft recoverable errors (e.g. single event upsets) or permanent damage. A typical example of a soft error is a bit-flip in the registry of a pixel, which changes the configuration bits, randomly increasing or decreasing the pixel threshold. Since the threshold was chosen close to the noise floor, a decrease of the threshold would lead to the pixel going to noise. This is then recognizable by a pixel sending out a huge amount of data (continuously triggering its readout). Shifting the threshold to a higher value results in a pixel with less sensitivity to radiation, thus systematically measuring lower count rates. In both cases, the pixel affected causes a systematic deviation of the overall measured cluster rate and thus also of the luminosity measurement.

We define a noisy pixel as a pixel showing significant deviation ($5\,\sigma$) of its count rate compared to the overall detector count rate. Noisy pixel identification and exclusion was done separately for each 3 hour long data taking period. Figure 2 shows the number of noisy pixels per 3 hour data taking as a function of the start time. It was found that on average 20 (0.03 %, TPX3_4A) and 15 (0.02 %, TPX3_4B) pixels became corrupted within one data taking period. Excluded pixels are randomly distributed across the pixel matrix of the sensor. After resetting the matrix configuration, pixels identified as noisy were fully recovered (soft errors). Infrequently, peaks in the number of noisy pixels were found. These are correlated to noise appearance in two neighboring columns. Column noise always appears in a double-column structure, resembling the fact that two columns share the same registry.

In figure 3, the noisy pixel appearance is shown as a function of accumulated luminosity within the 3 hour long data taking period. The correlation factors 0.54 (TPX_4A, chip ID: J04-W0036) and 0.66 (TPX_4B, chip ID: I04-W0036) were found indicating moderate correlation. With the

2020 JINST 15 C01039

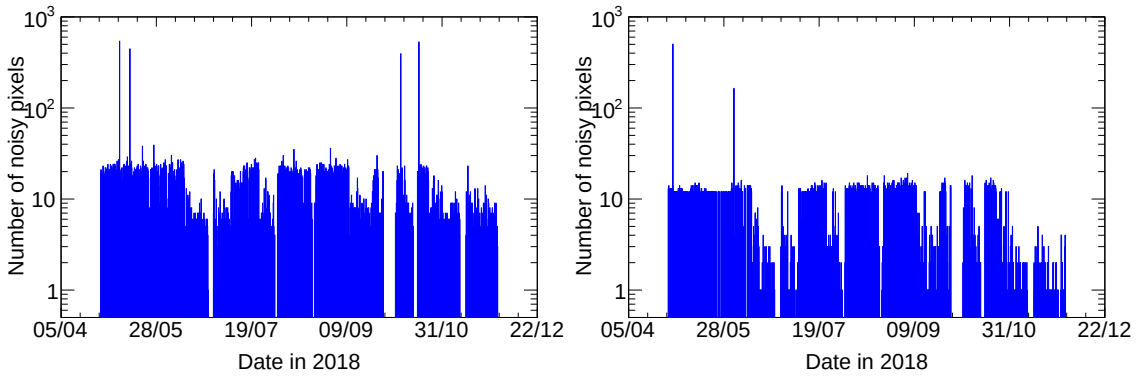

(a) TPX3_4A (J04-W0036) (b) TPX3_4B (I04-W0036)

Figure 2. Number of noisy pixels per 3 hour long data taking as a function of the start time.

luminosity to total ionizing dose (TID) conversion factor of $(4.44 \pm 0.54) \times 10^{-5} \frac{\text{Gy}}{\text{nb}^{-1}}$,[2] we estimate the maximal dose within a 3 hour period of $\text{TID}_{\text{max}} = (8.0 \pm 1.0)$ mGy. The total accumulated TID by the chips during their time of installation was $\text{TID}_{\text{total}} = (2.9 \pm 0.4)$ Gy. For the analyses in the following section noisy pixels were removed.

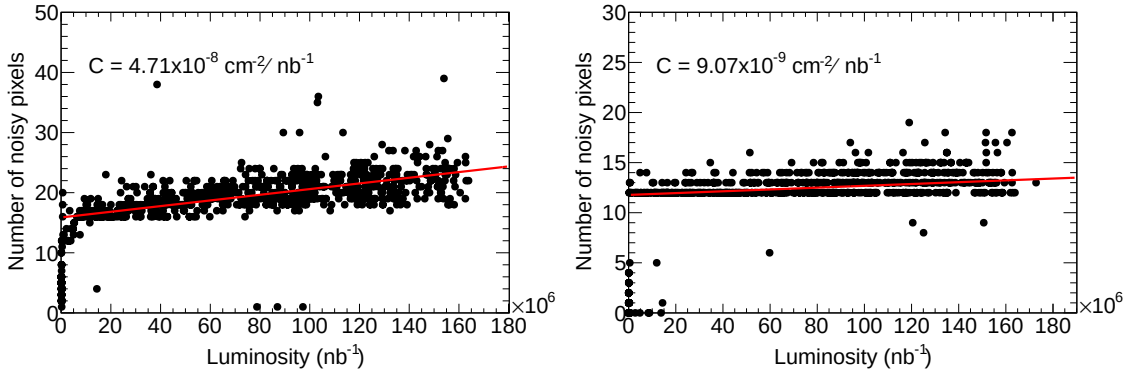

(a) TPX3_4A (J04-W0036) (b) TPX3_4B (I04-W0036)

Figure 3. Number of noisy pixels per 3 hour long data taking as a function of luminosity.

4 Relative luminosity measurement and achievable short-term relative precision

4.1 Cluster counting

Figure 4 shows the time integrated measured cluster counts as a function of the accumulated luminosity during an LHC fill in standard physics conditions.[3] It was found that, the measured count rate linearly increases with luminosity. A line fit to the data points gives the calibration factors

[2]Obtained from: https://twiki.cern.ch/twiki/bin/view/AtlasPublic/RadiationSimulationPublicResults.

[3]The luminosity measured by the Tile calorimeter was used [19].

2020 JINST 15 C01039

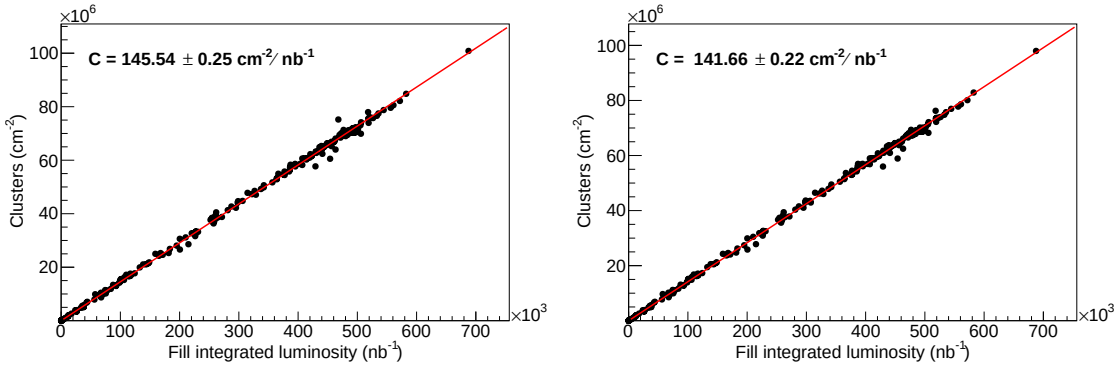

(a) TPX3_4A (J04-W0036)

(b) TPX3_4B (I04-W0036)

Figure 4. Scatter plot of the measured count rate as a function of luminosity. The Tile calorimeter luminosity measurement was used as a reference.

$C_{\text{clusters,I04}} = (141.7 \pm 0.2)\,\text{cm}^{-2}/\text{nb}^{-1}$ and $C_{\text{clusters,J04}} = (145.5 \pm 0.3)\,\text{cm}^{-2}/\text{nb}^{-1}$, which are used to determine the relative luminosity according to eq. (2.2).

Luminosity curve fitting. The measured temporal evolution of the luminosity is given for ATLAS Fill 6677 ($\mathcal{L} = 5.879 \times 10^5\,\text{nb}^{-1}$, peak luminosity $\mathcal{L}_{\text{peak}} = 2.1 \times 10^{34}\,\text{cm}^{-2}\text{s}^{-1}$) in figures 5(b) and 5(a). The number of protons in the bunch can be expressed as [16, 20]:

$$N_{\text{p}}(t) = N_0 \frac{e^{-\lambda_{\text{g}} t}}{1 + \frac{\lambda_{\text{bb}}}{\lambda_{\text{g}}}(1 - e^{-\lambda_{\text{g}} t})}. \tag{4.1}$$

λ_{g} denotes the losses of the bunch population due to the scattering of the beam with residual gas in the beam pipe, λ_{bb} denotes the losses due to beam-beam interactions and N_0 denotes the initial bunch population. Since $\mathcal{L}(t) \propto N_1(t)N_2(t)$, the luminosity curve can be described by [20]:

$$\mathcal{L}(t) = \mathcal{L}_0 \frac{e^{-2\lambda_{\text{g}}(t-t_0)}}{\left[1 + \frac{\lambda_{\text{bb}}}{\lambda_{\text{g}}}(1 - e^{-\lambda_{\text{g}}(t-t_0)})\right]^2}, \tag{4.2}$$

where $\mathcal{L}_0$ stands for the initial luminosity at the start of the decay t_0. Observed dips in the luminosity curve are due to tuning of the accelerator.

To determine the achievable short-term relative precision, eq. (4.2) was fitted to the measured data. Since a simultaneous fit of λ_{g} and λ_{bb} resulted in unphysical values, λ_{bb} was calculated according to [16]:

$$\lambda_{\text{bb}} = \frac{1}{t_{\text{bb}}^{\text{inel.}}} = \frac{N_{\text{exp.}} \times \sigma_{\text{inel.}} \times \mathcal{L}_0}{N_{\text{b}} \times N_0}. \tag{4.3}$$

and used as a fixed input parameter. With the number of colliding bunches $N_{\text{b}} = 2544$,[4] the initial number of protons per bunch $N_0 = 1.15 \times 10^{11}$, the inelastic cross section $\sigma_{\text{inel.}} = 80\,\text{mb}$, the number

[4]The values can be found at http://acc-stats.web.cern.ch/acc-stats/#lhc/overview-panel.

2020 JINST 15 C01039

of experiments $N_{\mathrm{exp}} = 2$ (ATLAS and CMS) and the luminosity at fill start $\mathcal{L}_0 \approx 19.4\,\mathrm{nb}^{-1}\mathrm{s}^{-1}$, we find:

$$\lambda_{\mathrm{bb}} = 0.91\,\mathrm{day}^{-1}. \tag{4.4}$$

Separate fits were done for each time period i between two consecutive accelerator tunings. Hereby, λ^i_{bb} was calculated by taking the luminosity dependence into account $\lambda^i_{\mathrm{bb}} = \sqrt{\mathcal{L}^i_0/\mathcal{L}_0} \times \lambda_{\mathrm{bb}}$. $\mathcal{L}^i_0$ was extracted from the measured data. The resulting fits are shown in figures 5(a) and 5(b). The fit parameters are tabulated in appendix A. Figures 5(d) and 5(c) show the distribution of the fit residuals. Their dispersion is described by Gaussian distributions, whose widths $\sigma_{\mathrm{res.,J4}} = 0.38\,\%$ and $\sigma_{\mathrm{res.,I4}} = 0.41\,\%$ indicate the achievable short-term relative precision. The width of the pull distributions in figures 5(f) and 5(e), $\sigma_{\mathrm{pull,J4}} = 1.33$ and $\sigma_{\mathrm{pull,I4}} = 1.32$, indicate the presence of systematic uncertainties.

4.2 Thermal neutron counting

Interaction of ions and neutrons with nuclei leads to the creation of radioactive isotopes in the surrounding of the detectors. This so-called induced radioactivity [2] is not only of concern for radiation protection but also adds unwanted signal to the Timepix3 luminosity measurement. The measured count rates of isotopes with short half life quickly saturate during collisions and quickly decay after collision, so that their effect is accounted for by the calibration factors. However, isotopes with a long half-life do not have enough time between collisions to decay so that they create an arbitrary offset to the luminosity value. The count rates from induced radioactivity can either be modeled (see e.g. [4, 5]) or excluded at the cost of lower statistical precision by using track properties. In the following section, we use the second approach. Induced radioactivity counts are neglected by considering only thermal neutrons, whose signatures can be separated reliably from electrons and γ-ray signatures [12].

In figure 6, the thermal neutron fluxes, determined according to eq. (2.1), are given as a function of luminosity. The calibration factor was found to be $C_{\mathrm{therm.}} = (1,036.16 \pm 0.09)\,\mathrm{cm}^{-2}/\mathrm{nb}^{-1}$. Figure 7(a) shows the luminosity curve determined from the thermal neutron fluxes. Using the fitting procedure described in section 4.1, the short-term relative precision $\sigma_{\mathrm{res.}} = 2.16\,\%$ and the width of the pull distribution $\sigma_{\mathrm{pull}} = 1.02$ were found. The pull width being close to 1 indicates that statistics is the limiting factor for increasing the measurement precision. The resulting fit parameters are tabulated in appendix B.

5 Summary and discussion

The following section summarizes the results shown above and discusses them in view of an upgrade of the Timepix network to a Timepix3 system for Run-3.

A method for identification and exclusion of noisy pixel was described. Noisy pixels are excluded for each data taking period separately. On average $\approx 0.03\,\%$ of the pixels were identified as suspicious. Such pixels could be recovered by reconfiguring the device, no pixel became permanently unusable. Moderate correlation of the number of noisy pixels to luminosity was found. Since noisy pixels create a huge amount of data, for future upgrade and the use in places

2020 JINST 15 C01039

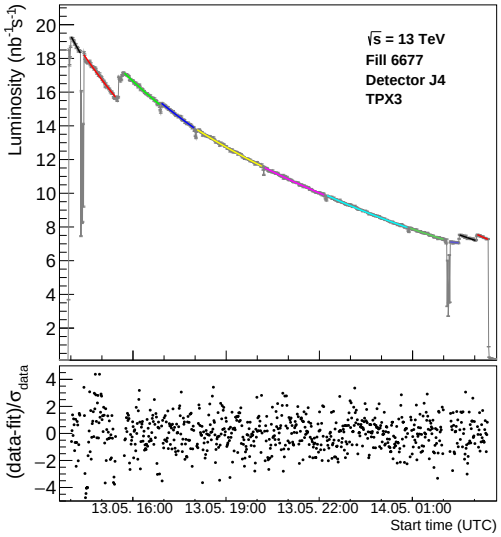

(a) TPX3_4A (J04-W0036)

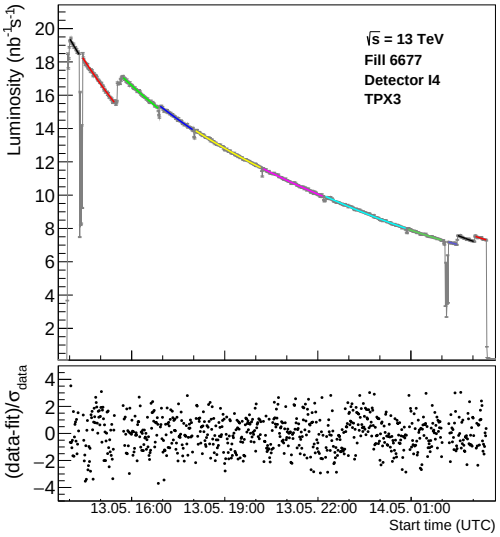

(b) TPX3_4B (I04-W0036)

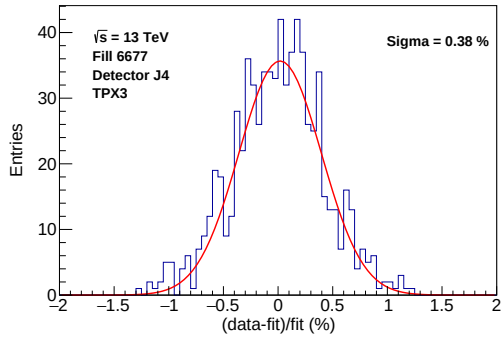

(c) TPX3_4A (J04-W0036): fit residuals

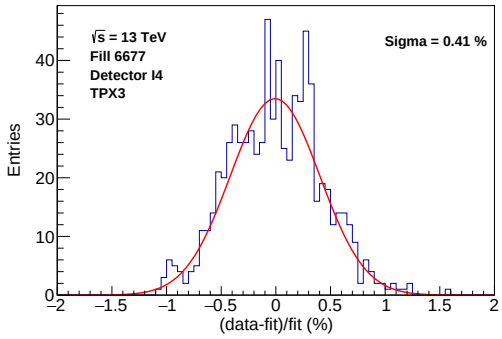

(d) TPX3_4B (I04-W0036): fit residuals

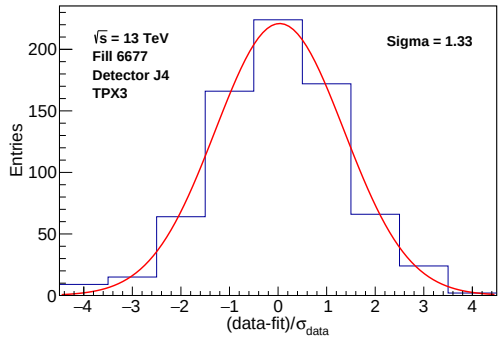

(e) TPX3_4A (J04-W0036): pull distribution

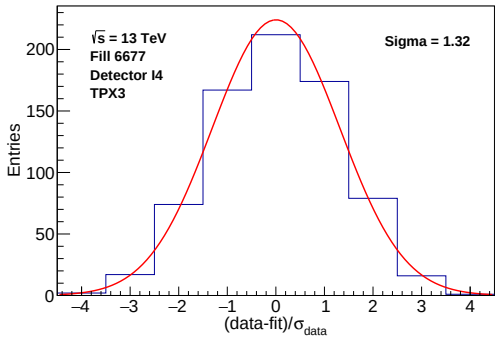

(f) TPX3_4B (I04-W0036): pull distribution

Figure 5. (a), (b): measured luminosity curve with a model fit to the data for ATLAS Fill 6677 ($\mathcal{L} = 5.879 \times 10^5\,\mathrm{nb}^{-1}$, $\mathcal{L}_{\mathrm{peak}} = 2.1 \times 10^{34}\,\mathrm{cm}^{-2}\mathrm{s}^{-1}$) on May 13–14, 2018. The time binning is 60 s; (c), (d): distribution of the fit residuals for estimation of the achievable short-term relative precision; (e), (f): pull distributions.

2020 JINST 15 C01039

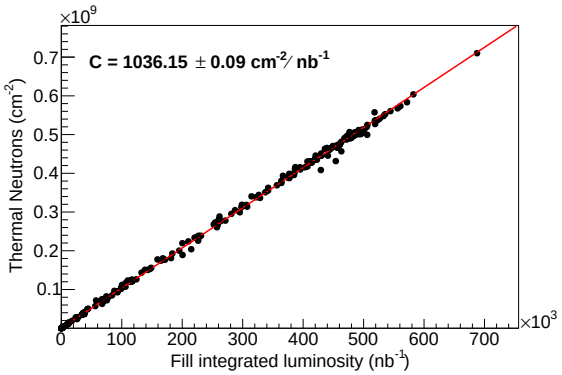

Figure 6. Measured thermal neutron fluence as a function of the fill integrated luminosity. The Tile calorimeter luminosity was used as a reference.

with higher radiation levels, noisy pixel removal should be done prior to data saving. Hereby, the simplicity of the presented algorithm allows for implementation in a microprocessor or FPGA.[5]

Table 2 gives an overview of the results presented in section 4. A short-term relative precision of $\leq 0.5\,\%$ was achieved in 60 s long time intervals using the overall cluster hit rates. The width of the pull distribution for cluster counting indicates the presence of systematic effects. With the number of cluster $N_{\text{clusters}} \geq 280$ per nb^{-1}, approximately 35 nb^{-1} are needed to achieve a relative statistical uncertainty of the luminosity measurement $\left(\frac{\Delta\mathcal{L}_{\text{TPX3}}}{\mathcal{L}_{\text{TPX3}}}\right)_{\text{stat.}}$ of less than 1 %. Using thermal neutrons (representing a subset of the overall cluster rate, selected by morphology and position in the pixel matrix) for luminosity determination, a precision of $\approx 2\,\%$ was achieved. In this case, statistics was the limiting factor. With $N_{\text{HB,LiF}} = 8$ per nb^{-1}, $N_{\text{Si}} = 2$ per nb^{-1} (see table 2) and eq. (2.1), $\approx 2,780$ nb^{-1} are needed to achieve a statistical precision of 1 %.

Table 2. Overview of the calibration factors, the achievable precision and the width of the pull distributions for the different methods discussed in the presented work.

Method (detector)	C (cm^{-2}/nb^{-1})	$N_{\text{event}}/\mathcal{L}$ (1/nb^{-1})	$\sigma_{\text{res.}}$(%)	σ_{pull}
Cluster counting (TPX_4A)	145.5 ± 0.3	288	0.39	1.27
Cluster counting (TPX_4B)	141.7 ± 0.2	282	0.41	1.27
Therm. neut. counting (TPX_4B)	1, 036.15 ± 0.09	8 (^{6}LiF), 2 (Si)	2.16	1.02

When compared with results of the detector previously installed at the same position, TPX04 (Timepix network), an increased sensitivity was found ($C_{\text{clusters,TPX04}} = 43.6\,\text{cm}^{-2}/\text{nb}^{-1}$ for the 300 µm thick layer 1 and $C_{\text{clusters,TPX04}} = 50.6\,\text{cm}^{-2}/\text{nb}^{-1}$ for the 500 µm thick layer 2, see TABLE I in [21]). This increase is related to the lower detection threshold in combination with the reduced track overlap and reduced dead times in Timepix3. Whereas TPX04 was not used for precision analysis of luminosity, the newly added Timepix3 device shows promising results. Higher statistical accuracy can be achieved by increasing the amount of sensors in the current position or by going closer to the interaction point. It was shown in [16] that a precision of $\approx 0.1\,\%$ can be achieved

[5]Field programmable gate array.

2020 JINST 15 C01039

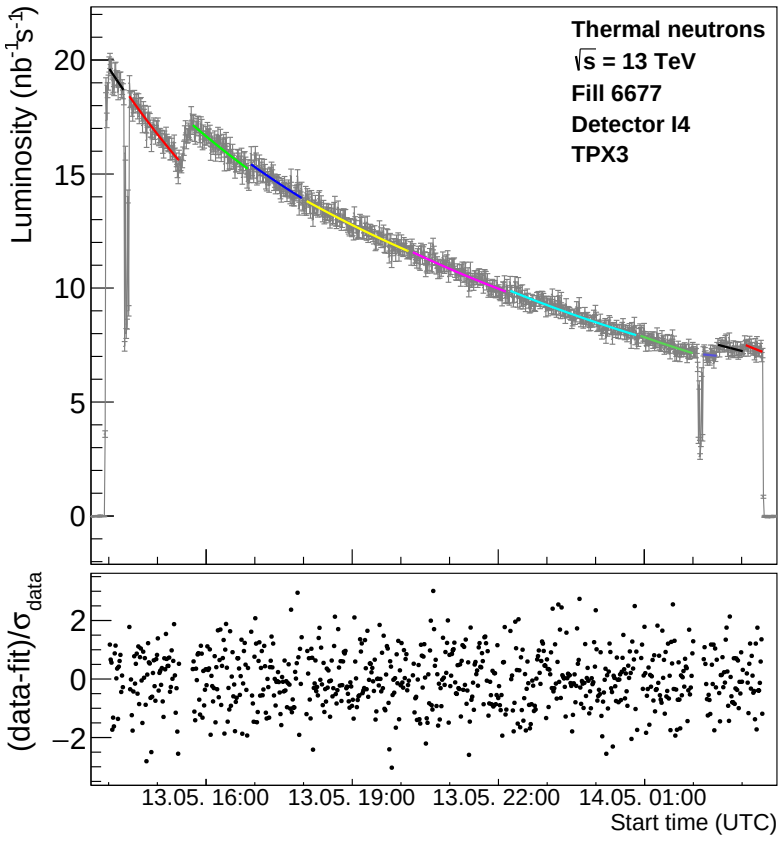

(a)

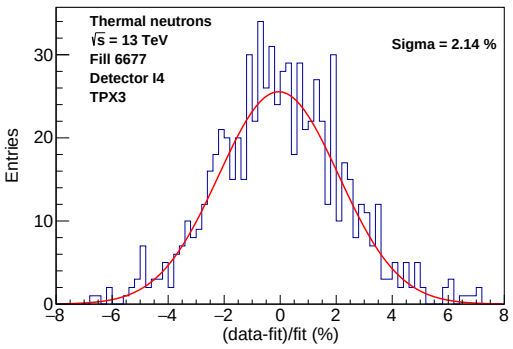

(b) Thermal neutrons: fit residuals

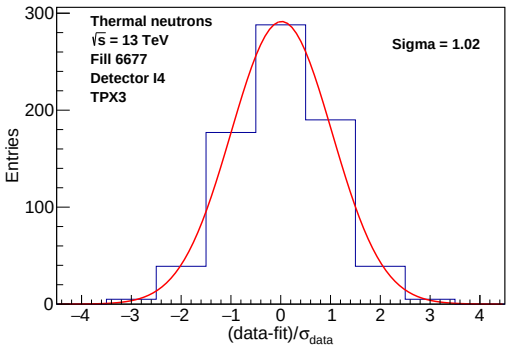

(c) Thermal neutrons: pull distribution

Figure 7. (a) Luminosity curve determined with thermal neutron counting with a model fit for ATLAS Fill 6677 ($\mathcal{L} = 5.879 \times 10^5\,\mathrm{nb}^{-1}$, $\mathcal{L}_{\mathrm{peak}} = 2.1 \times 10^{34}\,\mathrm{cm}^{-2}\mathrm{s}^{-1}$) on May 13-14, 2018. (b) Distribution of the fit residuals; (c) Pull distribution for the thermal neutron measurement.

2020 JINST 15 C01039

using the hit counting method with Timepix devices closer to the interaction point. With Timepix3 devices and cluster counting in similar positions, at least the same precision can be expected. The higher radiation levels closer to the interaction point come with an increased probability of radiation damage, which manifests itself e.g. by an increased leakage current or a reduced detector efficiency. The impact of the former effect can be suppressed by setting a per-pixel threshold level far above the noise floor. The latter effect can be recognized (and corrected for) by comparing the fill integrated luminosities of the inner and outer detectors in the Timepix(3) network.

Future work of Timepix3 data evaluation focuses on modeling and subtracting of activation from the cluster count rate, studying the capabilities of Timepix3 to assign the luminosity to each individual bunch (bunch crossing identification BCID) and to do absolute luminosity measurements.

Acknowledgments

We thank the Medipix collaboration for the development of the Timepix3 ASIC and ATLAS for providing the Tile luminosity values. The work was further supported by the European Regional Development Fund-Projects "Van de Graaff Accelerator — a Tunable Source of Monoenergetic Neutrons and Light Ions" (No. CZ.02.1.01/0.0/0.0/16_013/0001785), "Engineering applications of physics of microworld" (No. CZ.02.1.01/0.0/0.0/16_019/0000766), and the Ministry of Education, Youth and Sports of the Czech Republic under "RICE — New Technologies and Concepts for Smart Industrial Systems", project No. LO1607.

A Tabulated fit values: cluster counting

Table 3. Overview of the luminosity curve fit parameters for the cluster counting method. λ_{bb} was calculated and used as input paramter.

	TPX_4A (J04-W0036)			**TPX_4B (I04-W0036)**		
Fit	$\mathcal{L}_0$ (nb^{-1})	λ_g (10^{-5}s^{-1})	λ_{bb} (10^{-5}s^{-1})	$\mathcal{L}_0$ (nb^{-1})	λ_g (10^{-5}s^{-1})	λ_{bb} (10^{-5}s^{-1})
0	19.3 ± 0.02	1.42 ± 0.10	1.05	19.4 ± 0.02	1.26 ± 0.103	1.05
1	18.2 ± 0.01	1.04 ± 0.012	1.02	18.3 ± 0.01	1.18 ± 0.016	1.02
2	17.1 ± 0.01	0.454 ± 0.014	0.988	17.1 ± 0.01	0.447 ± 0.014	0.986
3	15.3 ± 0.01	0.416 ± 0.016	0.935	15.3 ± 0.01	0.363 ± 0.017	0.935
4	13.8 ± 0.007	0.293 ± 0.0063	0.887	13.9 ± 0.007	0.303 ± 0.0063	0.89
5	11.5 ± 0.007	0.319 ± 0.0078	0.811	11.6 ± 0.007	0.331 ± 0.0078	0.813
6	9.88 ± 0.006	0.439 ± 0.0054	0.751	9.93 ± 0.006	0.439 ± 0.0055	0.753
7	7.93 ± 0.008	0.472 ± 0.022	0.672	7.95 ± 0.008	0.437 ± 0.022	0.673
8	7.19 ± 0.007	0.834 ± 0.11	0.637	7.18 ± 0.01	0.35 ± 0.168	0.64
9	7.53 ± 0.01	0.559 ± 0.070	0.655	7.57 ± 0.01	0.653 ± 0.071	0.657
10	7.55 ± 0.01	0.913 ± 0.13	0.656	7.52 ± 0.01	0.488 ± 0.129	0.655

2020 JINST 15 C01039

B Tabulated fit values: thermal neutron counting

Table 4. Overview of the luminosity curve fit parameters for the thermal neutron counting method.

TPX_4B (I04-W0036)			
Fit	$\mathcal{L}_0$ (nb^{-1})	λ_g (10^{-5}s^{-1})	λ_{bb} (10^{-5}s^{-1})
0	19.6 ± 0.167	1.26 ± 0.717	1.06
1	18.4 ± 0.0845	1.28 ± 0.11	1.03
2	17.2 ± 0.0765	0.502 ± 0.0966	0.989
3	15.4 ± 0.0764	0.427 ± 0.116	0.938
4	13.8 ± 0.0515	0.303 ± 0.0444	0.888
5	11.6 ± 0.0491	0.394 ± 0.0549	0.813
6	9.89 ± 0.0394	0.468 ± 0.0386	0.751
7	7.91 ± 0.0543	0.654 ± 0.155	0.672
8	7.15 ± 0.0495	0.600 ± 0.400	0.636
9	7.51 ± 0.0785	0.388 ± 0.494	0.654
10	7.5 ± 0.096	0.979 ± 0.907	0.654

References

[1] C. Leroy et al., *Proposal to Measure Radiation Field Characteristics, Luminosity and Induced Radioactivity in ATLAS with TIMEPIX Devices*, Project Proposal, 2014.

[2] M. Campbell, E. Heijne, C. Leroy, M. Nessi, S. Pospisil, J. Solc et al., *Induced radioactivity in ATLAS cavern measured by MPX detector network*, 2019 *JINST* **14** P03010.

[3] ATLAS collaboration, *The ATLAS Experiment at the CERN Large Hadron Collider*, 2008 *JINST* **3** S08003.

[4] ATLAS collaboration, *Analysis of the Radiation Field in ATLAS Using 2008 2011 Data from the ATLAS-MPX Network*, ATL-GEN-PUB-2013-001 (2013).

[5] A. Sopczak, B. Ali, J. Begera, B. Bergmann, T. Billoud, B. Biskup et al., *Precision measurements of induced radioactivity and absolute luminosity determination with TPX detectors in LHC proton–proton collisions at 13 TeV*, *IEEE Trans. Nucl. Sci.* **65** (2018) 1371.

[6] B. Bergmann, T. Billoud, C. Leroy and S. Pospisil, *Characterization of the radiation field in the ATLAS experiment with timepix detectors*, *IEEE Trans. Nucl. Sci.* **66** (2019) 1861.

[7] T. Poikela, J. Plosila, T. Westerlund, M. Campbell, M. De Gaspari, X. Llopart, et al., *Timepix3: a 65K channel hybrid pixel readout chip with simultaneous ToA/ToT and sparse readout*, 2014 *JINST* **9** C05013.

[8] P. Burian, P. Broulím, B. Bergmann, V. Georgiev, S. Pospíšil, L. Pušman et al., *Timepix3 detector network at ATLAS experiment*, 2018 *JINST* **13** C11024.

[9] ATLAS collaboration, *Luminosity determination in pp collisions at $\sqrt{s}$ = 8 TeV using the ATLAS detector at the LHC*, *Eur. Phys. J.* **C 76** (2016) 653 [arXiv:1608.03953].

2020 JINST 15 C01039

[10] J. Jakubek, *Precise energy calibration of pixel detector working in time-over-threshold mode*, *Nucl. Instrum. Meth.* **A 633** (2011) S262.

[11] B. Bergmann, M. Pichotka, S. Pospisil, J. Vycpalek, P. Burian, P. Broulim et al., *3D track reconstruction capability of a silicon hybrid active pixel detector*, *Eur. Phys. J.* **C 77** (2017) 421.

[12] B. Bergmann, I. Caicedo, C. Leroy, S. Pospisil and Z. Vykydal, *ATLAS-TPX: a two-layer pixel detector setup for neutron detection and radiation field characterization*, 2016 *JINST* **11** P10002.

[13] B. Bergmann, R.O. Nelson, J.M. O'Donnell, S. Pospisil, J. Solc, H. Takai et al., *Time-of-flight measurement of fast neutrons with Timepix detectors*, 2014 *JINST* **9** C05048.

[14] T. Holy, E. Heijne, J. Jakubek, S. Pospisil, J. Uher and Z. Vykydal, *Pattern recognition of tracks induced by individual quanta of ionizing radiation in Medipix2 silicon detector*, *Nucl. Instrum. Meth.* **A 591** (2008) 287.

[15] P. Francavilla, *The ATLAS tile hadronic calorimeter performance at the LHC*, *J. Phys. Conf. Ser.* **404** (2012) 012007.

[16] A. Sopczak, B. Ali, T. Asawatavonvanich, J. Begera, B. Bergmann, T. Billoud et al., *Precision luminosity of LHC proton–proton collisions at 13 TeV using hit counting with TPX pixel devices*, *IEEE Trans. Nucl. Sci.* **64** (2017) 915.

[17] S. van der Meer, *Calibration of the effective beam height in the ISR*, CERN-ISR-PO-68-31 (1968).

[18] N. Asbah, *LHC luminosity measurement with the ATLAS-MPX detectors*, MSc Thesis, Département de physique Faculté des arts et des sciences, Université de Montréal (2013).

[19] ATLAS collaboration, *Luminosity determination in pp collisions at* $\sqrt{s} = 13$ *TeV using the ATLAS detector at the LHC*, ATLAS-CONF-2019-021 (2019).

[20] A. Sopczak, B. Ali, N. Asbah, B. Bergmann, K. Bekhouche, D. Caforio et al., *MPX detectors as LHC luminosity monitor*, *IEEE Trans. Nucl. Sci.* **62** (2015) 3225.

[21] A. Sopczak, *Timepix3 luminosity determination of 13 TeV proton-proton collisions at the ATLAS experiment*, *IEEE Trans. Nucl. Sci.* (2020) 1.

2020 JINST 15 C01039